Fusion reactions in multicomponent dense matter

D. G. Yakovlev
Ioffe Physico-Technical Institute, Poliekhnicheskaya 26, RU-194021 Saint Petersburg, Russia and Department of Physics & Joint Institute for Nuclear Astrophysics, University of Notre Dame, Notre Dame, Indiana 46556, USA

L. R. Gasques
Department of Physics & The Joint Institute for Nuclear Astrophysics, University of Notre Dame, Notre Dame, Indiana 46556, USA

A. V. Afanasjev
Department of Physics and Astronomy, Mississippi State University, P.O. Drawer 5167, Mississippi 39762-5167, USA

M. Beard and M. Wiescher
Department of Physics & The Joint Institute for Nuclear Astrophysics, University of Notre Dame, Notre Dame, Indiana 46556 USA
(Received 13 March 2006; published 27 September 2006)

We analyze thermonuclear and pycnonuclear fusion reactions in dense matter containing atomic nuclei of different types. We extend a phenomenological expression for the reaction rate, proposed recently by Gasques *et al*. [Phys. Rev. C **72**, 025806 (2005)] for the one-component plasma of nuclei, to the multicomponent plasma. The expression contains several fit parameters which we adjust to reproduce the best microscopic calculations available in the literature. Furthermore, we show that pycnonuclear burning is drastically affected by an (unknown) structure of the multicomponent matter (a regular lattice, a uniform mix, etc.). We apply the results to study nuclear burning in a ^{12}C-^{16}O mixture. In this context, we present new calculations of the astrophysical S factors for carbon-oxygen and oxygen-oxygen fusion reactions. We show that the presence of a C-O lattice can strongly suppress carbon ignition in white dwarf cores and neutron star crusts at densities $\rho \gtrsim 3 \times 10^9$ g cm^{-3} and temperatures $T \lesssim 10^8$ K.

DOI: 10.1103/PhysRevC.74.035803 PACS number(s): 25.60.Pj, 26.50.+x, 97.10.Cv

I. INTRODUCTION

Nuclear reactions are very important in the physics of stars. They determine hydrogen burning in main-sequence stars, helium burning in red giants, and carbon, neon, and oxygen burning at later stages. They determine also nucleosynthesis in shock-driven stellar explosions, such as type II supernovae, as well as ignition and burning in accreting stars.

Steady-state and explosive thermonuclear carbon burning during late stellar evolution [1] and in shock fronts of type II supernovae [2] is governed by the ^{12}C+^{12}C and possibly by the ^{12}C+^{16}O fusion processes. Similarly, thermonuclear oxygen burning is mainly determined by the ^{16}O+^{16}O and possibly by the ^{16}O+^{20}Ne reactions [3]. The ignition and nucleosynthesis that occur during these burning phases critically depend on the initial fuel abundance and thermonuclear reaction rates.

In high-density cores of white dwarfs and crusts of neutron stars, thermonuclear reactions are strongly affected by plasma effects (which are especially important for carbon ignition in cores of accreting massive white dwarfs for triggering type Ia supernova explosions). The ignition conditions are sensitive to the ^{12}C and ^{16}O abundance and to the fusion reaction rates [4].

Carbon ignition has also been suggested as a trigger of superbursts in surface layers of accreting neutron stars [5]. However, the required ignition conditions seem to disagree with the observed superburst light curves [6]. Alternative explanations are presently being discussed, such as carbon ignition in the crust of an accreting strange (quark) star, to accommodate the observed light-curve characteristics [7]. While in most of the scenarios pure carbon burning dominates energy production, the presence of other elements affects ignition conditions and associated nucleosynthesis.

Pycnonuclear burning occurs in dense and cold cores of white dwarfs [8] and in crusts of accreting neutron stars [9,10]. Theoretical formalism has been developed mostly for pycnonuclear reactions between equal nuclei, but one often needs to consider multicomponent matter, for instance, carbon-oxygen cores of white dwarfs.

In a previous publication [11], we focused on fusion reactions between equal nuclei in a one-component plasma (OCP) of atomic nuclei (ions). In the present work, we expand the study toward a multicomponent plasma (MCP). The problem has two aspects; the first one is associated with the underlying nuclear physics, while the second one is concerned with the plasma physics. The nuclear part deals with the reliable determination of astrophysical S factors at stellar energies. These energies are low (typically lower than a few MeV), in particular if compared to the presently accessible range of low-energy fusion experiments. This prevents direct measurements of S factors at laboratory conditions. Thus, one needs to calculate the S factors theoretically and use these results to extrapolate measured S factors toward a lower stellar energy range. In Sec. II, we present calculations of the S factors for the two reactions of astrophysical importance, ^{12}C+^{16}O and ^{16}O+^{16}O.

The plasma physics problem consists of calculating the Coulomb barrier penetration in nuclear reactions taking into account the Coulomb fields of surrounding plasma particles.

These fields modify the reaction rates and lead to five nuclear burning regimes [8] (two thermonuclear regimes, with weak and strong plasma screening; two pycnonuclear regimes for zero-temperature and thermally enhanced burning; and the intermediate regime). These regimes are described in Sec. III; their validity conditions are specified in Sec. III A. In ordinary stars, nuclear burning proceeds in the weak screening thermonuclear regime [12,13]. The foundation of the theory of thermonuclear burning with strong plasma screening was laid by Salpeter [14]. The strict theory of pycnonuclear burning was developed by Salpeter and Van Horn [8]. References to other works can be found in Sec. III and in [11].

In Sec. III, we analyze calculations of Coulomb barrier penetration in MCP and propose a phenomenological expression for a reaction rate valid in all five regimes for any nonresonant fusion reaction. This expression accurately reproduces well-known results in thermonuclear regimes and gives a reasonable description of the Coulomb tunneling problem in other regimes. It is important to incorporate plasma physics effects into computer codes which simulate nucleosynthesis, especially at high densities in compact stars such as white dwarfs and neutron stars (see above). In Sec. IV, we illustrate the results of Secs. II and III by analyzing nuclear burning in ^{12}C-^{16}O mixtures, with the emphasis on the carbon ignition curve.

II. ASTROPHYSICAL *S* FACTORS FOR CARBON-OXYGEN MIXTURES

To study nuclear burning in dense stellar carbon-oxygen matter (Sec. IV), we need fusion cross sections (or associated astrophysical factors) for three reactions: ^{12}C+^{12}C, ^{12}C+^{16}O, and ^{16}O+^{16}O. For calculating the cross sections, we employ the one-dimensional barrier penetration (BP) formalism [15] and adopt the São Paulo potential [16–19] to describe the real part of the nuclear interaction $V_N(r, E)$:

$$V_N(r, E) = V_{\rm SP}(r, E) = V_F(r) \exp\left(-4{\rm v}^2/c^2\right). \quad (1)$$

Here, $V_F(r)$ is the density-dependent double-folding potential, c is the speed of light, E is the particle collision energy (in the center-of-mass reference frame), v is the local relative velocity of two nuclei 1 and 2,

$${\rm v}^2(r, E) = (2/\mu)[E - V_C(r) - V_N(r, E)], \quad (2)$$

$V_C(r)$ is the Coulomb potential, and μ is the reduced mass.

In this paper, we adopt the two-parameter Fermi (2pF) distribution to describe the nuclear densities. The radii of these distributions are well approximated by the formula $R_0 = 1.31A^{1/3} - 0.84$ fm [19]. The ^{12}C and ^{16}O diffuseness was taken to be 0.56 and 0.58 fm, respectively. These values were extracted from heavy-ion elastic scattering data at subbarrier and intermediate energies, by applying an unfolding method involving the São Paulo potential (see Refs. [20–22] for details).

Usually, fusion cross sections $\sigma(E)$ at low energies, typical for astrophysical conditions, are expressed in terms of the astrophysical S factor

$$S(E) = \sigma(E)E \exp(2\pi\eta), \quad (3)$$

where $\eta = (Z_1 Z_2 e^2/\hbar)\sqrt{\mu/(2E)}$ is the familiar Gamow parameter; Z_1 and Z_2 are charge numbers of the nuclei. This parametrization removes from the fusion cross section the strong nonnuclear energy dependence [13,23] associated with Coulomb barrier penetration. If $S(E)$ is a slowly varying function of E, it can be extrapolated to the lower energies relevant to stellar burning.

The S factors for all three reactions versus E are shown in the upper panels of Fig. 1. Solid lines are theoretical

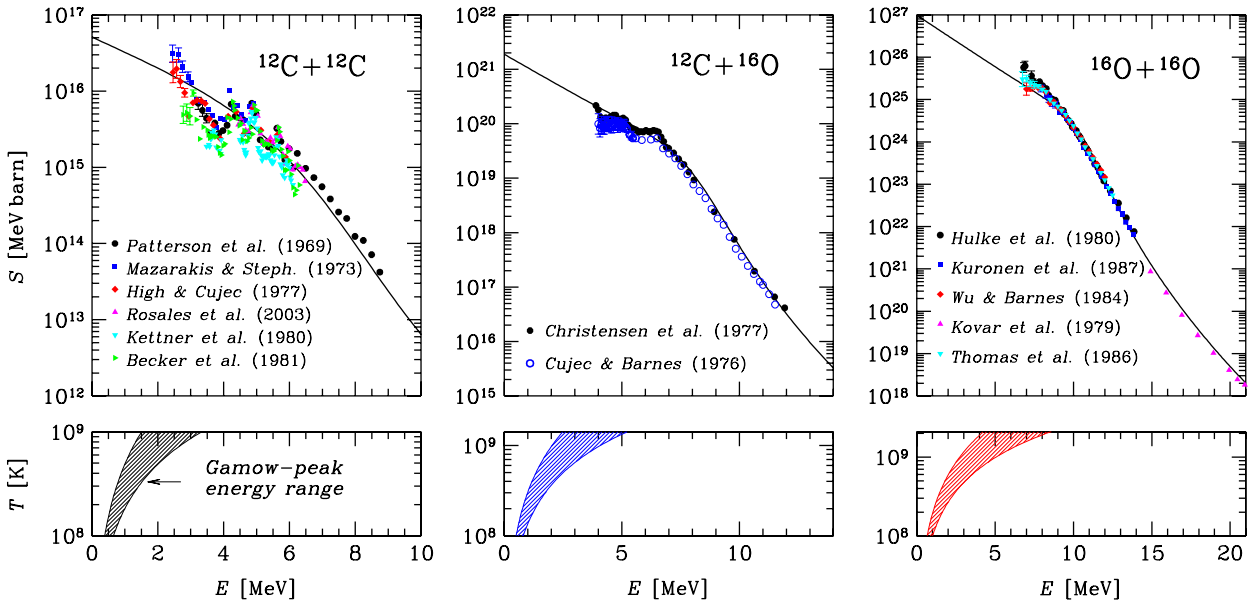

FIG. 1. (Color online) Top: Astrophysical S factors as a function of the center-of-mass energy E for the ^{12}C+^{12}C, ^{12}C+^{16}O, and ^{16}O+^{16}O reactions. Solid lines correspond to the BP model calculations; various symbols are experimental data. Bottom: Gamow-peak energy ranges for these reactions in the thermonuclear regime vs temperature T of stellar matter. See text for details.

calculations using the BP model, while symbols are experimental data. The results for the C+C reaction have already been discussed in Ref. [11] and are presented here for completeness of consideration. The data for this reaction are taken from Patterson *et al.* [24], Mazarakis and Stephens [25], High and Cujec [26], Rosales *et al.* [27], Kettner *et al.* [28], and Becker *et al.* [29]. The data for the C+O reaction are taken from Christensen *et al.* [30] and Cujec and Barnes [31]. Finally, the data for the O+O reaction are from Hulke *et al.* [32], Kuronen *et al.* [33], Wu and Barnes [34], Kovar *et al.* [35], and Thomas *et al.* [36]. Lower panels in Fig. 1 show the Gamow-peak energy ranges versus the temperature of stellar matter in the thermonuclear burning regime; they will be discussed in Sec. III A.

The sub-Coulomb-barrier resonances exhibited in the C+C data at $E \lesssim 6$ MeV and in the C+O data at $E \lesssim 7.7$ MeV cannot be reproduced in the framework of the BP model. However, the model provides an average description of the light- and heavy-ion fusion at energies below and above the barrier. Depending on the nuclear potential, it also gives a satisfactory parameter-free description of the energy dependence of the S factor, which seems reasonably accurate for extrapolating the experimental data into the stellar energy range.

The data sets presented by the different groups are not in perfect agreement. For instance, the two C+O data sets agree in average, but disagree within a factor of ~2 for lowest E. The overall agreement between the theory and the data is ~50%. However, in the low-energy region, the slope of the measured cross section reported in Ref. [30] does not follow the calculated S factors. It is difficult to predict where the data will lie in the energy range $E \lesssim 4$ MeV. Regarding the O+O reaction, the discrepancies between the different experimental results at sub-barrier energies are around a factor of 3. The overall agreement between the data and the theory is ~30%. At the lowest measured energy, the data and the theory differ by at most a factor of 3. Further experiments at lower energies would help verify the validity of the predicted fusion cross sections. Nevertheless, it is important to highlight that the BP model does not contain any free parameter. In this sense, the S factor calculations do not represent a fit to the experimental data and can be considered as a useful tool for predicting the average nonresonant low-energy cross sections for a wide range of fusion reactions. For many astrophysical reactions, such a description gives a reasonable estimate because the formalism of stellar reaction rates relies on the S factor averaged over an entire Gamow-peak range.

The values of $S(E)$ calculated up to $E \leqslant 20$ MeV can be fitted by the analytic expression

$$S(E) = \exp\left(A_1 + A_2\,\Delta E + \frac{A_3 + A_4\,\Delta E + A_5\,\Delta E^2}{1 + \exp[-\Delta E]}\right) \text{MeV b}, \qquad (4)$$

where $\Delta E = E - E_0$; the center-of-mass energy E and the fit parameter E_0 are expressed in MeV. Table I gives the fit parameters $A_1, \ldots, A_5$ and E_0 for the C+C, C+O, and O+O reactions. The maximum formal fit errors are 7.2% at $E =$ 19.8 MeV for C+C; 6.3% at $E = 7.5$ MeV for C+O; and 3.9% at $E = 8.2$ MeV for the O+O reaction. The S factor for the C+C reaction was fitted in a previous paper [11] by a slightly different expression with approximately the same accuracy. We have fitted the same data by the new expression (4) for completeness of consideration. The two fits are nearly equivalent.

TABLE I. Coefficients $A_1, \ldots, A_5$ and E_0 in the fits expression (4) for the S factors of the C+C, C+O, and O+O reactions.

Reaction	E_0	A_1	A_2	A_3	A_4	A_5
^{12}C+^{12}C	6.946	34.75	−0.552	−2.131	−0.625	0.0315
^{12}C+^{16}O	8.290	44.32	−0.561	−1.480	−0.910	0.0387
^{16}O+^{16}O	10.52	56.16	−0.571	−1.160	−1.044	0.0366

III. NUCLEAR FUSION RATE

A. Physical conditions and reaction regimes

Let us consider a stellar matter which consists of ions and electrons. We assume that the ions are fully ionized and the electrons form a uniform electron background. We study a multicomponent mixture of ion species $j = 1, 2, \ldots,$ with atomic numbers A_j and charge numbers Z_j. Let n_j be the number density of ions j. The total number density of ions is $n = \sum_j n_j$; the electron number density is $n_e = \sum_j Z_j n_j$. For an OCP of ions, the index j will be omitted. The number density n_j can be expressed through the mass density ρ of the matter as $n_j = X_j \rho/(A_j m_u)$, where X_j is the mass fraction of ions j, and $m_u = 1.66055 \times 10^{-24}$ g is the atomic mass unit. In a not too dense matter, the total mass fraction contained in the nuclei is $X_N = \sum_j X_j \approx 1$. At densities higher than the neutron drip density (~4×10^{11} g cm^{-3}), the matter also contains free neutrons; the total mass fraction contained in the nuclei is then $X_N < 1$. It is also useful to introduce the fractional number $x_j = n_j/n$ of nuclei j among other nuclei, with $\sum_j x_j = 1$. Generally,

$$n_e = n\langle Z\rangle, \qquad \rho = \frac{m_u n \langle A\rangle}{X_N}, \quad x_j = \frac{X_j/A_j}{\sum_i X_i/A_i},$$
$$\langle Z\rangle = \sum_j x_j Z_j, \quad \langle A\rangle = \sum_j x_j A_j, \qquad (5)$$

where $\langle Z\rangle$ and $\langle A\rangle$ are the mean charge and mass number of ions, respectively.

Let us also introduce the Coulomb coupling parameter Γ_j for ions j,

$$\Gamma_j = \frac{Z_j^2 e^2}{a_j k_B T} = \frac{Z_j^{5/3} e^2}{a_e k_B T},$$
$$a_e = \left(\frac{3}{4\pi n_e}\right)^{1/3}, \quad a_j = Z_j^{1/3} a_e, \qquad (6)$$

where T is the temperature, k_B is the Boltzmann constant, a_e is the electron-sphere radius, and a_j is the ion-sphere radius (a radius of a sphere around a given ion, where the electron charge compensates the ion charge). Therefore, Γ_j is the ratio of a typical electrostatic energy of the ion to the thermal energy.

If $\Gamma_j \ll 1$, then the ions constitute an almost ideal Boltzmann gas; while for $\Gamma_j \gtrsim 1$, they are strongly coupled by Coulomb forces (constituting either a Coulomb liquid or solid). The transformation from the gas to the liquid at $\Gamma_j \sim 1$ is smooth, without any phase transition. The solidification is realized as a weak first-order phase transition. According to highly accurate Monte Carlo calculations, a classical OCP of ions solidifies at $\Gamma \approx 175$ (see, e.g., Ref. [37]).

It is useful to introduce the mean ion coupling parameter $\langle\Gamma\rangle = \sum_j x_j \Gamma_j$. The plasma can be treated as strongly coupled if $\langle\Gamma\rangle \gtrsim 1$. This happens at $T \lesssim T_l$, where

$$k_B T_l = \sum_j \left(Z_j^2 e^2/a_j\right) x_j = k_B T \langle\Gamma\rangle. \tag{7}$$

For low temperatures $T \ll T_p \ll T_l$, ion motion can no longer be considered as classical but should be quantized. Here, T_p is the Debye (plasma) temperature associated with the ion plasma frequency ω_p (a typical frequency of ion vibrations in Coulomb crystals—see, e.g., Ref. [8]),

$$T_p = \frac{\hbar\omega_p}{k_B}, \quad \omega_p^2 = \sum_j \frac{4\pi Z_j^2 e^2 n_j}{A_j m_u}. \tag{8}$$

The most difficult problem posed by a strongly coupled MCP at low temperatures is understanding its actual state. Extensive Monte Carlo simulations [38] of the freezing of a classical OCP indicate that it can freeze into imperfect body-centered cubic (bcc) or faced-centered cubic (fcc) microcrystal (or microcrystals). Unfortunately, publications on reliable simulations of freezing of an MCP are almost absent. Evidently, the cold MCP is much more rich in physics than the OCP. It can be an MCP regular lattice or microcrystals (with defects); an amorphous, uniformly mixed structure; or a lattice of one phase with random admixture of other ions. One cannot exclude an ensemble of phase-separated domains. For the sake of completeness, we will consider different possibilities. An MCP obeys the linear mixing rule with high accuracy. Accordingly, the difference in energies of the indicated states is very small and is a subject of vigorous debates (e.g., Ref. [39] and references therein). It is possible that a low-temperature MCP can be in different states depending on the history of its formation in a star with decreasing temperature.

To make our consideration less abstract, we will apply it to a ^{12}C-^{16}O mixture. The appropriate temperature-density diagram is shown in Fig. 2. We present the temperatures T_l, T_m, and T_p for a pure carbon matter ($x_C = 1$, solid lines), for a mixture of equal amounts of C and O nuclei ($x_C = \frac{1}{2}$, long dashes) and for a pure oxygen matter ($x_C = 0$, short dashes). The melting temperature of the C-O mixture is taken to be $T_m = T_l/175$. The plasma temperature T_p is the same for all three cases. Notice that the electrons are strongly degenerate at all ρ and T displayed in Fig. 2. At $\rho > 4 \times 10^{10}$ g cm^{-3}, carbon nuclei cannot survive in dense matter because of β captures; at $\rho > 2 \times 10^{10}$ g cm^{-3}, oxygen nuclei will also be destroyed by β captures. Therefore, it is unreasonable to extend the C-O diagram to higher densities.

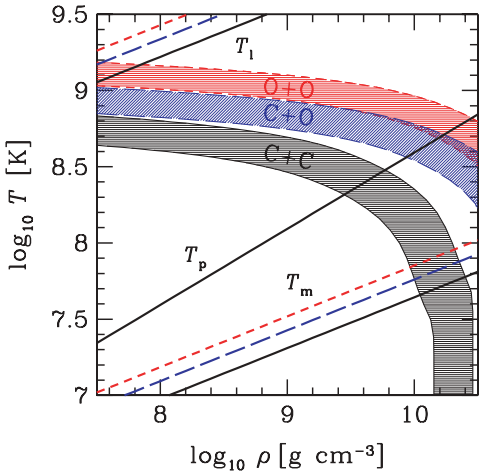

FIG. 2. (Color online) Temperature-density diagram for ^{12}C-^{16}O matter. Straight lines show temperature T_l of the appearance of ion liquid, melting temperature T_m of ion crystal, and ion plasma temperature T_p. Solid lines refer to pure carbon matter, long dashes to C-O matter with equal particle fractions of C and O, and short dashes to pure oxygen matter. Three shaded strips show the regions important for C+C burning (in pure carbon matter), C+O burning (in C-O mixture), and O+O burning (in pure oxygen matter). Each strip is restricted by upper and lower lines along which the burning time equals 1 year and 10^6 years, respectively (see the text for details).

We will be interested in nuclear fusion reactions

$$(A_i, Z_i) + (A_j, Z_j) \to (A_c, Z_c), \tag{9}$$

where $A_c = A_i + A_j$ and $Z_c = Z_i + Z_j$ refer to a compound nucleus c. For our example in Fig. 2, we have three reactions, C+C, C+O, and O+O (Sec. II). The experimental cross sections for these reactions show no pronounced resonance structures and can be described in the framework of nonresonant reaction formalism [11,23] as discussed above. Notice that the data for the C+C and C+O reactions exhibit some resonant structures demonstrated in Fig. 1. In the lower panel of this figure, we show the Gamow-peak energy range as a function of temperature for these reactions in the thermonuclear burning regime (Sec. III B). We see that at high enough T, the Gamow-peak range covers the energy range where the oscillations are experimentally measured. However, at these values of T, the Gamow-peak range is sufficiently wide, and the energy integration in the reaction rate should smear out the oscillatory behavior. For lower T, the Gamow peak is narrower, but it shifts to low energies inaccessible to laboratory experiments. In the absence of experimental and theoretical data on the presence of oscillations at these low energies, we will adopt the standard assumption that the reactions in question can be treated as nonresonant in applications to stellar burning.

The shaded strips in Fig. 2 show the T-ρ domains most important for these reactions. We will describe them in more detail in Sec. IV.

To study a reaction (9) we introduce the so called ion-sphere quantities

$$a_{ij} = \frac{a_i + a_j}{2}, \quad \Gamma_{ij} = \frac{Z_i Z_j e^2}{a_{ij} k_B T}, \quad T_{ij}^{(l)} = \frac{Z_i Z_j e^2}{a_{ij} k_B},$$
$$T_{ij}^{(p)} = \frac{\hbar}{k_B}\left(\frac{4\pi Z_i Z_j e^2 n_{ij}}{2\mu_{ij}}\right)^{1/2}, \tag{10}$$

where $\mu_{ij} = m_u A_i A_j / A_c$ is the reduced mass of the reacting nuclei, and $n_{ij} = 3/(4\pi a_{ij}^3)$. Basing on the ion-sphere model of a strongly coupled Coulomb plasma, one expects (e.g., Ref. [40]) that a_{ij} characterizes an equilibrium distance between neighboring nuclei i and j, Γ_{ij} describes their Coulomb coupling, $T_{ij}^{(l)}$ is the temperature for the onset of strong coupling, and $T_{ij}^{(p)}$ is a local Debye temperature (for oscillations of ions i and j). In an OCP, we have $a_{ij} = a$, $\Gamma_{ij} = \Gamma$, $T_{ij}^{(p)} = T_p$. We will also need

$$r_{Bij} = \hbar^2/(2\mu_{ij} Z_i Z_j e^2), \tag{11}$$

which reduces to the ion Bohr radius in the case of equal ions $j = i$. In addition, we will need the parameter

$$\lambda_{ij} = r_{Bij}\left(\frac{n_{ij}}{2}\right)^{1/3} = \frac{2r_{Bij}}{\left(Z_i^{1/3} + Z_j^{1/3}\right)}\left(\frac{\rho X_N \langle Z\rangle}{2\langle A\rangle m_u}\right)^{1/3}$$
$$= \frac{A_i + A_j}{A_i A_j Z_i Z_j \left(Z_i^{1/3} + Z_j^{1/3}\right)} \times \left(\frac{\rho X_N \langle Z\rangle}{\langle A\rangle\ 1.3574 \times 10^{11}\ \mathrm{gcm}^{-3}}\right)^{1/3}, \tag{12}$$

which corresponds to the parameter λ introduced by Salpeter and Van Horn [8] in the OCP case.

In the following sections, we will discuss nuclear burning in MCP for the five burning regimes introduced in Ref. [8] and analyzed in detail for OCP in our previous work [11]. We will demonstrate that the formalism developed for OCP can be adapted to more complex MCP scenarios.

B. Classical thermonuclear reaction rate

In the classical thermonuclear (weak screening) regime ($T \gg T_{ij}^{(l)}$) the reacting ions constitute an almost ideal gas [12]. The rate for nonresonant fusion processes (such as considered here) is well known as

$$R_{ij}^{\mathrm{th}} = \frac{4 n_i n_j}{1 + \delta_{ij}} \sqrt{\frac{2E_{ij}^{\mathrm{pk}}}{3\mu_{ij}}} \frac{S\left(E_{ij}^{\mathrm{pk}}\right)}{k_B T} \exp(-\tau_{ij}), \tag{13}$$

where $S(E)$ is the astrophysical factor; δ_{ij} is the Kronecker delta, which excludes double counting of the same collisions in reactions with identical nuclei ($i = j$); $E_{ij}^{\mathrm{pk}} = T k_B \tau_{ij}/3$ is the Gamow-peak energy (the relative energy of colliding nuclei which gives the major contribution into the reaction rate) and

$$\tau_{ij} = \left(\frac{27\pi^2 \mu_{ij} Z_i^2 Z_j^2 e^4}{2 k_B T \hbar^2}\right)^{1/3} \tag{14}$$

is the parameter which characterizes the Coulomb barrier penetrability. This parameter can be written as

$$\tau_{ij} = 3(\pi/2)^{2/3}\left(E_{ij}^{\mathrm{a}}/k_B T\right)^{1/3}, \quad E_{ij}^{\mathrm{a}} \equiv 2\mu_{ij} Z_i^2 Z_j^2 e^4/\hbar^2. \tag{15}$$

Then

$$R_{ij}^{\mathrm{th}} = \frac{n_i n_j}{1 + \delta_{ij}} S\left(E_{ij}^{\mathrm{pk}}\right) \frac{r_{Bij}}{\hbar} P_{\mathrm{th}} F_{\mathrm{th}}, \tag{16}$$

where r_{Bij} is a convenient dimensional factor defined by Eq. (11), F_{th} is the exponential function, and P_{th} is the pre-exponent, that is,

$$F_{\mathrm{th}} = \exp(-\tau_{ij}), \quad P_{\mathrm{th}} = \frac{8\pi^{1/3}}{\sqrt{32}^{1/3}}\left(\frac{E_{ij}^{a}}{k_B T}\right)^{2/3}. \tag{17}$$

Typically, the main contribution into the reaction rate comes from suprathermal particles ($E_{ij}^{\mathrm{pk}} \gg k_B T$), and the Coulomb barrier is very thick ($\tau_{ij} \gg 1$). The reaction rate decreases exponentially with decreasing T. Typical Gamow-peak energy ranges for the C+C, C+O, and O+O reactions in the thermonuclear regimes are shown in Fig. 1. These energies are defined as $E_{ij}^{\mathrm{pk}} - \Delta E \lesssim E \lesssim E_{ij}^{\mathrm{pk}} + \Delta E$, with $\Delta E \sim 2\sqrt{E_{ij}^{\mathrm{pk}} k_B T}$.

C. Thermonuclear regime with strong screening

The thermonuclear regime with strong plasma screening operates in the temperature range $T_{ij}^{(p)} \lesssim T \lesssim T_{ij}^{(l)}$, where the plasma ions constitute a strongly coupled Coulomb system (liquid or solid). The majority of ions are confined in deep Coulomb potential wells, but the main contribution into the reaction rate comes from a very small amount of highly energetic suprathermal ions which are nearly free (see, e.g., Refs. [8,14]). However, neighboring plasma ions strongly screen the Coulomb interaction between the reacting ions. The screening simplifies close approaches of the reacting ions, required for a Coulomb tunneling, and thus enhances the reaction rate (with respect to the classical thermonuclear reaction rate).

In analogy with the OCP case (e.g., Ref. [11]), the enhancement can be included in the exponential function

$$F_{\mathrm{th}} = F_{\mathrm{sc}} \exp(-\tau_{ij}), \quad F_{\mathrm{sc}} = \exp(h_{ij}), \tag{18}$$

where F_{sc} is the enhancement factor and h_{ij} is a function of plasma parameters.

We will analyze h_{ij} in the same manner as was done in Ref. [11] for the OCP. For this purpose, we notice that the reacting nuclei move in the potential $W(r) = Z_i Z_j e^2/r - H_{ij}(r)$, where $H_{ij}(r)$ is the plasma potential created by neighboring plasma ions. In the thermonuclear regime, $H_{ij}(r)$ is almost constant along a Coulomb tunneling path. Accordingly, h_{ij} can be split into two terms, $h_{ij} = h_{ij}^{(0)} + h_{ij}^{(1)}$. The main term $h_{ij}^{(0)}$ is obtained assuming that $H_{ij}(r) \approx H_{ij}(0)$ is constant along a tunneling path; a small correction $h_{ij}^{(1)}$ is produced by a weak variation of the plasma potential along this path. We will discuss $h_{ij}^{(0)}$ explicitly in this section and introduce

$h_{ij}^{(1)}$ phenomenologically in Sec. III G, when we propose an analytic approximation for the reaction rate in all regimes.

It is well known (e.g., Refs. [14,41]) that $h_{ij}^{(0)} = H_{ij}(0)/k_BT$, where $H_{ij}(0)$ is the properly averaged (mean-field) plasma potential at $r = 0$. Thus defined, $H_{ij}(0)$ becomes a thermodynamic quantity which can be expressed through the difference of the classical Coulomb free energies for a given system and for a system with the two reacting nuclei merging into a compound nucleus (e.g., Ref. [41]). However, a strongly coupled classical multicomponent Coulomb liquid obeys very accurately the linear mixing rule (see Ref. [39] for recent results). Using this rule, one obtains

$$h_{ij}^{(0)} = f_0(\Gamma_i) + f_0(\Gamma_j) - f_0(\Gamma_c), \tag{19}$$

where $f_0(\Gamma)$ is the Coulomb free energy per ion in an OCP (in units of k_BT). This formula was derived by Jancovici [42] for an OCP and generalized by Mochkovitch for an MCP (see Ref. [43]). The function $f_0(\Gamma)$ is very accurately determined by Monte Carlo simulations. For instance, according to DeWitt and Slattery [44], the function $f_0(\Gamma)$ for a classical one-component Coulomb liquid at $1 \leqslant \Gamma \leqslant 170$ can be approximated as

$$\begin{aligned} f_0(\Gamma) = &-0.899172\Gamma + (1/s)0.602249\,\Gamma^s \\ &- 0.274823\ln\Gamma - 1.401915, \end{aligned} \tag{20}$$

where $s = 0.3230064$. It gives a highly accurate expression for $h_{ij}^{(0)}$, but it is inconvenient for an analytic interpolation of the reaction rate (Sec. III G). Instead, we will use a simpler linear expression $f_0(\Gamma) = -0.9\,\Gamma$ provided by the ion-sphere model [14],

$$\begin{aligned} h_{ij}^{(0)} &= C_{ij}^{\rm sc}\,\Gamma_{ij}, \\ C_{ij}^{\rm sc} &= 0.9\left[Z_c^{5/3} - Z_i^{5/3} - Z_j^{5/3}\right]\frac{Z_i^{1/3} + Z_j^{1/3}}{2Z_iZ_j}. \end{aligned} \tag{21}$$

This expression seems crude, but it is actually accurate. For a nuclear reaction in an OCP ($Z_i = Z_j = Z_c/2$), this equation gives $C^{\rm sc} = 1.0573$, very close to the value 1.0754 inferred [11] from Eq. (20). In the range of $1 \leqslant \Gamma_{ij} \leqslant 170$, the ion-sphere model (21) gives the enhancement factor $\exp(h_{ij}^{(0)})$ which is systematically lower than the more accurate enhancement factor, given by Eqs. (19) and (20). The maximum difference in these enhancement factors for charge ratios $1/5 \leqslant Z_i/Z_j \leqslant 5$ reaches $\approx$15 at the highest value of $\Gamma_{ij} = 170$. This difference can be regarded as insignificant because at such Γ_{ij} the enhancement factor itself is as huge as $\exp(h_{ij}^{(0)}) \sim 10^{74}$. For lower Γ_{ij}, the expression (21) is more accurate. For instance, for $\Gamma_{ij} = 50$ and $Z_i/Z_j = 5$, it underestimates the enhancement factor by only a factor of 3. In the range of $1 \leqslant \Gamma_{ij} \leqslant 10$ for $1/5 \leqslant Z_i/Z_j \leqslant 5$, the underestimation does not exceed a factor of 1.5. Notice that in the MCP, the factor $C_{ij}^{\rm sc}$ depends on Z_i and Z_j.

Although the above approach is more accurate, one usually calculates $h_{ij}^{(0)}$ by extrapolating the mean-field plasma potential $H_{ij}(r)$, obtained from classical Monte Carlo sampling, to $r \to 0$. In particular, Ogata *et al.* [45,46] used this method to study the enhancement of thermonuclear burning in the liquid phases of OCP and binary ion mixtures (BIMs). The leading term in Eqs. (19) and (20) of Ref. [46], equivalent to the leading terms (19) and (21), is $h_{ij}^{(0)} = \Gamma_{ij}(1.148 - 0.00944\ln\Gamma_{ij} - 0.000168\,(\ln\Gamma_{ij})^2)$. This expression was employed also by Kitamura [47] for constructing the analytic approximation for the reaction rates in OCP and BIMs in all reaction regimes (although by that time a more accurate expression was obtained by Ogata [48] for the OCP using path integral Monte Carlo simulations). Comparing the expression of Ref. [46] with (19) and (21) we see that the expression of Ref. [46] systematically overestimates the plasma enhancement. In the OCP, the overestimation reaches [11] a factor of $\sim$40 for $\Gamma = 170$, which is not very significant. However, the coefficients in this expression are independent of Z_i and Z_j, in disagreement with Eq. (21). As a result, the overestimation increases with the growth of the charge ratio Z_i/Z_j, reaching $\sim$150 and $\sim 2\times10^4$ at $Z_i/Z_j = 2$ and $Z_i/Z_j = 5$, respectively, for $\Gamma_{ij} = 170$. Therefore, when the difference of charges Z_i and Z_j increases, the results of Refs. [46] and [47] become less accurate. The inaccuracy comes from the problem of extrapolating $H_{ij}(r)$ to $r \to 0$. This inaccuracy was analyzed by Rosenfeld for the OCP [49] and the MCP [50].

Equations (20) and (21) become invalid in the regime of weak screening ($\Gamma_{ij} \ll 1$; Sec. III B), where the well-known Debye-Hückel theory should be used. In particular, the screening function in the weakly coupled MCP becomes [14]

$$h_{ij}^{(0)} = \frac{Z_iZ_je^2}{k_BTr_D} = \left(\frac{3\Gamma_e^3\langle Z^2\rangle Z_i^2Z_j^2}{\langle Z\rangle}\right)^{1/2}, \tag{22}$$

where r_D is the ion Debye screening length and $\langle Z^2\rangle \equiv \sum_j Z_j^2x_j$. Introducing Γ_{ij}, we obtain

$$h_{ij}^{(0)} = \zeta_{ij}\Gamma_{ij}^{3/2}, \quad \zeta_{ij} = \left(\frac{3\langle Z^2\rangle\left(Z_i^{1/3} + Z_j^{1/3}\right)^3}{8\langle Z\rangle Z_iZ_j}\right)^{1/2}. \tag{23}$$

For reactions in an OCP, we have $\zeta = \sqrt{3}$. In an MCP, ζ_{ij} depends on ion charge numbers.

A simple phenomenological interpolation which reproduces the strong and weak screening limits [Eqs. (21) and (23)] and combines them in the Γ_{ij} range from $\sim$0.1 to $\sim$1 is

$$h_{ij}^{(0)} = C_{ij}^{\rm sc}\Gamma_{ij}^{3/2}\Big/\left[\left(C_{ij}^{\rm sc}/\zeta_{ij}\right)^4 + \Gamma_{ij}^2\right]^{1/4}. \tag{24}$$

Because accurate calculations of the MCP free energy of ions in this range are absent, we cannot test the accuracy of our interpolation. However, the plasma screening enhancement of reaction rates at these values of Γ_{ij} is weak, and the interpolation uncertainty does not strongly affect the reaction rates.

D. Zero-temperature pycnonuclear regime

This regime operates at low temperatures, $T \lesssim 0.5T_{ij}^{(p)}/\ln(T_{ij}^{(l)}/T_{ij}^{(p)})$, at which thermal effects are negligible and all the ions occupy ground states in their potential wells. The Coulomb barrier is penetrated owing to zero-point vibrations of ions around their equilibrium positions. Because the

vibration amplitudes are generally small, neighboring pairs of ions (closest neighbors) make the major contribution to the reaction rate.

Generalizing Eq. (35) of Salpeter and Van Horn [8] to the MCP case, we can present the pycnonuclear reaction rate as [see, e.g., Eq. (7) in Ref. [45]]

$$R_{ij}^{\rm pyc} = \frac{n_i}{1+\delta_{ij}} \langle \nu_{ij} p_{ij} \rangle_{\rm av}, \tag{25}$$

where ν_{ij} is the number of nearest nuclei j around a nucleus i, p_{ij} is the reaction rate for a fixed pair ij, and the brackets $\langle \ldots \rangle_{\rm av}$ denote statistical averaging over an ensemble of such pairs. For instance, it is currently thought that the OCP of ions at zero temperature forms a bcc crystal. In this case, any ion is surrounded by its eight closest neighbors, with the equilibrium distance between them $d = (3\pi^2)^{1/6} a$, where a is the ion-sphere radius.

According to Eqs. (35), (37), and (39) of Ref. [8], the reaction rate for a pair of neighboring ions in an OCP can be written as

$$p = D_{\rm pyc} \frac{\lambda^{3-C_{\rm pl}} S(E^{\rm pk})}{\hbar r_B^2} \exp\left(-\frac{C_{\rm exp}}{\sqrt{\lambda}}\right), \tag{26}$$

where λ and r_B are given by Eqs. (12) and (11), respectively (for the OCP); while $D_{\rm pk}$, $C_{\rm pl}$, and $C_{\rm exp}$ are constants which depend on a Coulomb barrier penetration model and on the lattice type. Finally, the characteristic reaction energy is $E^{\rm pk} \sim \hbar\omega_p = k_B T_p$, where ω_p is the ion plasma frequency defined by Eq. (8) (a typical frequency of zero-point ion vibrations).

Salpeter and Van Horn [8] used the WKB approximation and considered two models of Coulomb barrier penetration in the bcc lattice—the static and relaxed lattice models—to account for the lattice response to a motion of tunneling nuclei. Later Schramm and Koonin [9] extended this consideration taking into account the dynamic effect of motion of surrounding ions in response to the motion of the tunneling nuclei in the relaxed lattice. In addition, they considered the fcc Coulomb lattice. The results of Refs. [8,9] are analyzed in Ref. [11]. Note that the pycnonuclear burning rates for fcc or bcc OCP crystals are very similar. We expect that for an amorphous OCP they are of the same order of magnitude.

Pycnonuclear reactions in the MCP require complicated calculations (which, hopefully, will be done in the future). We will restrict ourselves to a simpler consideration based on similarity criteria and some general assumptions. Even the state of the MCP at low temperatures is not clear. For example, it can be a regular lattice (with defects), a uniformly mixed state, an ensemble of phase-separated domains, etc. (Sec. III A). It can also be a combination of these states.

1. Uniformly mixed MCP

Let us start with a uniformly mixed MCP. An obvious generalization of Eq. (26) to the MCP would be to replace $r_B \to r_{Bij}$ and $\lambda \to \lambda_{ij}$ in accordance with Eqs. (11) and (12). This replacement should correctly reflect the rescaling of inter-ion distances and oscillator frequencies in an MCP within the ion-sphere model (see, e.g., Ref. [51]).

However, the rescaling may be not exact. We will take this into account by adopting a simplified assumption that any pair of close neighbors behaves as *an elementary oscillator* with an equilibrium separation d_{ij} and an oscillator frequency ω_{ij}. For an OCP, we have $\lambda \sim \hbar^2/(A m_u d^2 \omega)^2$ and $\omega \sim \omega_p$. In the MCP, we expect to have $\lambda \to \widetilde{\lambda}_{ij} \sim \hbar^2/(2\mu_{ij} d_{ij}^2 \omega_{ij})^2$, where d_{ij} and ω_{ij} are the actual equilibrium distance and the effective oscillator frequency, respectively. With this replacement from Eq. (26), we obtain

$$p_{ij} = D_{\rm pyk} \frac{\widetilde{\lambda}_{ij}^{3-C_{\rm pl}} S(E_{ij}^{\rm pk})}{\hbar r_{Bij}^2} \exp\left(-\frac{C_{\rm exp}}{(\widetilde{\lambda}_{ij})^{1/2}}\right). \tag{27}$$

Now we assume that the actual values d_{ij} and ω_{ij} can deviate from the ion-sphere values $d_{ij}^{(0)}$ and $\omega_{ij}^{(0)}$ and introduce the quantities

$$\alpha_{dij} = d_{ij}/d_{ij}^{(0)}, \qquad \alpha_{\omega ij} = \omega_{ij}/\omega_{ij}^{(0)}, \tag{28}$$

which measure the deviations. They will be treated as parameters to be varied within reasonable limits. Then

$$\widetilde{\lambda}_{ij} = \lambda_{ij}\alpha_{\lambda ij}, \qquad \alpha_{\lambda ij} \equiv 1/\left(\alpha_{dij}^4 \alpha_{\omega ij}^2\right), \tag{29}$$

where λ_{ij} is given by Eq. (12).

Another way to improve the ion-sphere rescaling for a pycnonuclear reaction in a BIM was proposed by Ichimaru *et al.* [51], who used the formal relation $\lambda_{ij} \sim r_{Bij}/d_{ij}$ and suggested that $\widetilde{\lambda}_{ij} = \lambda_{ij}/\alpha_{dij}$, which corresponds to $\alpha_{\lambda ij} = 1/\alpha_{dij}$. Therefore, they allowed d_{ij} to be different from $d_{ij}^{(0)}$ but assumed that the oscillator frequency ω_{ij} adjusts to this new separation following the ion-sphere rescaling, so that $\alpha_{\omega ij}^2 = 1/\alpha_{dij}^3$. In contrast, we allow the separations and oscillator frequencies to deviate independently, and our consideration is more general.

Following Ogata *at al.* [45] [see their Eq. (7)], we assume that the number of closest neighbors j around the ion i in Eq. (25) is $\langle \nu_{ij} \rangle_{\rm av} = 8 n_j/n$ (which is appropriate for a uniform mix). The factor 8 may be approximate, but it affects only the pre-exponent of the reaction rate, which is much less significant than the exponentially small probability of Coulomb tunneling. Substituting (27) and (28) into (25), we obtain

$$R_{ij}^{\rm pyc} = D_{\rm pyc} \frac{4 n_i n_j}{1+\delta_{ij}} \frac{8\langle Z \rangle}{\left(Z_i^{1/3} + Z_j^{1/3}\right)^3} \frac{S(E_{ij}^{\rm pk})}{\hbar} \times \frac{r_{Bij}}{\widetilde{\lambda}_{ij}^{C_{\rm pl}}} \exp\left(-\frac{C_{\rm exp}}{(\widetilde{\lambda}_{ij})^{1/2}}\right). \tag{30}$$

This equation has the same structure as Eq. (16) and can be written as

$$R_{ij}^{\rm pyc} = \frac{n_i n_j}{1+\delta_{ij}} S(E_{ij}^{\rm pk}) \frac{r_{Bij}}{\hbar} P_{\rm pyc} F_{\rm pyc}, \tag{31}$$

with

$$P_{\rm pyc} = \frac{8\langle Z \rangle}{\left(Z_i^{1/3} + Z_j^{1/3}\right)^3} \frac{4 D_{\rm pyc}}{\widetilde{\lambda}_{ij}^{C_{\rm pl}}}, \qquad F_{\rm pyc} = \left(-\frac{C_{\rm exp}}{(\widetilde{\lambda}_{ij})^{1/2}}\right). \tag{32}$$

TABLE II. Coefficients in the interpolation expressions for a reaction rate for the optimal model of nuclear burning and for the models which maximize and minimize the rate. The parameters $C_T, \alpha_{\lambda ij}, \alpha_{\omega ij}$ are different for MCP and OCP (the values for OCP [11] are given in parentheses). For an MCP, the models assume a uniformly mixed state (see the text for details).

Model	$C_{\rm exp}$	$C_{\rm pyc}$	$C_{\rm pl}$	C_T	$\alpha_{\lambda ij}$	$\alpha_{\omega ij}$	Λ
Optimal	2.638	3.90	1.25	0.724 (0.724)	1 (1)	1 (1)	0.5
Maximum rate	2.450	50	1.25	0.840 (0.904)	1.05 (1)	0.95 (1)	0.35
Minimum rate	2.650	0.5	1.25	0.768 (0.711)	0.95 (1)	1.05 (1)	0.65

For numerical evaluations, we have

$$R_{ij}^{\rm pyc} = 10^{46} C_{\rm pyc} \frac{8\rho X_N x_i x_j A_i A_j \langle A\rangle Z_i^2 Z_j^2}{(1+\delta_{ij})A_c^2} S\left(E_{ij}^{\rm pk}\right) \times \widetilde{\lambda}_{ij}^{3-C_{\rm pl}} \exp\left(-\frac{C_{\rm exp}}{(\widetilde{\lambda}_{ij})^{1/2}}\right) {\rm cm}^{-3}{\rm s}^{-1}, \quad (33)$$

where $C_{\rm pyc} = D_{\rm pyc}/(8 \times 11.515)$; the density ρ is expressed in g cm^{-3} and the astrophysical factor $S(E_{ij}^{\rm pk})$ is in MeV barn. The reaction energy is $E_{ij}^{\rm pk} \sim \hbar\omega_{ij} = \alpha_{\omega ij} k_B T_{ij}^{(p)}$. The main parameter regulating the reaction rate is $\widetilde{\lambda}_{ij}$ in the exponent argument. For sufficiently low densities, $\widetilde{\lambda}_{ij}$ is very large, strongly suppressing the Coulomb tunneling. With growing ρ, the barrier becomes more transparent and the reaction rate increases.

For the OCP with $\alpha_\lambda = 1$, Eqs. (30)–(33) reduce to the well-known equations for zero-temperature pycnonuclear burning in a crystalline lattice. The constants $C_{\rm pyc}, C_{\rm pl}$, and $C_{\rm exp}$, obtained using various techniques, have been analyzed in Ref. [11]. In Table II, we present these parameters for three models. The first model is optimal (seems to be the most reliable). It is the static-lattice model of Salpeter and Van Horn [8] for the bcc crystal. The second and third models are phenomenological; they have been proposed in Ref. [11], basing on the results of Refs. [8,9,45,47]. The second model gives the upper limit of the reaction rate, and the third gives the lower limit (for both bcc and fcc crystals). We expect that the reaction rate in an amorphous OCP would lie within the same limits.

Returning to an MCP, we must additionally specify the scaling factor $\alpha_{\lambda ij}$ in Eq. (29). Some attempts have been made [45,51] to determine proper inter-ion separations d_{ij} (i.e., the values of α_{dij}) at $T = 0$ in BIM solids from positions of first correlation peaks in radial pair distribution functions of ions, $g_{ij}(r)$. These functions have been calculated by Monte Carlo sampling. Such studies require powerful computer resources and may be inconclusive at present. This is clearly seen from similar (and simpler) attempts of the same group [45,46,51,52] to determine deviations of inter-ion separations from the ion-sphere scaling in BIM liquids [using first-peak positions of $g_{ij}(r)$]. The authors applied their results to study an effect of these deviations on thermonuclear burning in the strong screening regime. Our analysis of those results shows that no statistically significant deviations from the ion-sphere scaling have been found (and no associated effects on nuclear burning can actually be predicted). This conclusion is strengthened by the critical analysis of these works by Rosenfeld [49,50]. Therefore, no reliable information has been obtained on the violation of the ion-sphere scaling of inter-ion separations in the BIM liquids and solids [on the level of a few percent, which is most likely the real uncertainty in the determination of $g_{ij}(r)$ peak positions in the cited publications].

Equally, proper oscillator frequencies ω_{ij} (and parameters $\alpha_{\omega ij}$) in BIMs could be determined from molecular dynamics simulations, but such simulations have not yet been performed.

In the absence of precise microscopic calculations of d_{ij} and ω_{ij}, we naturally assume that the optimal values are $\alpha_{dij} = \alpha_{\omega ij} = \alpha_{\lambda ij} = 1$. In order to maximize the reaction rate, we propose to increase $\alpha_{\lambda ij}$ (somewhat arbitrarily) by 5%, and in order to minimize the rate, we propose to reduce it by 5%. These proposed values are also listed in Table II. Notice that it is difficult to expect that the variations of α_{dij} and $\alpha_{\omega ij}$ in Eq. (28) are fully independent. An increase in the inter-ion separation d_{ij} should cause a decrease in the oscillator frequency ω_{ij}; these variations should be partially compensated in the factor $\alpha_{\lambda ij} = 1/(\alpha_{dij}^4 \alpha_{\omega ij}^2)$.

2. *Regular MCP lattice*

Now we turn to the case of a regular MCP lattice, which can be drastically different from a uniform mix. The central point is the availability of closest neighbors *ij*. If they are absent, the reaction (9) occurs via Coulomb tunneling of more distant *ij* pairs and becomes strongly suppressed.

The closest-neighbor condition depends on the crystal type. For instance, consider a binary bcc crystal composed of ions i and j. There are eight pairs of closest neighbors in a basic cubic cell (formed by one ion in the center of the cell and any other ion in a vertex). If all ions are of the same type (e.g., $x_i = 1$), then all eight pairs participate in the same reaction *ii* (the OCP case). In the BIM case ($x_i = x_j = \frac{1}{2}$), we have an ion i in the center of the cell and ions j in vertices, and all eight pairs of closest neighbors participate only in the reaction *ij*. The reactions *ii* and *jj* will be strongly blocked because any pairs *ii* and *jj* are not closest neighbors. Then the ion i in the center of the basic cell will be able to react with six ions i in centers of adjacent cells. The equilibrium distance between these pairs is a factor of $2/\sqrt{3} \approx 1.155$ larger than between the closest neighbors, which will exponentially suppress the *ii* reaction rate.

One can construct more complicated MCP lattice structures and formulate appropriate blocking conditions. The strongest blocking of pycnonuclear reactions is expected in a regular crystal with many components. In that case, the probability to find specified closed neighbors *ij* could be very selective.

3. *Other MCP structures*

If the matter consists of domains of separated phases, pycnonuclear burning occurs mainly within these domains.

The rate of the reaction ii in domains containing ions i can be calculated from Eq. (33), assuming OCP ($x_i = 1$), and then diluted by a volume fraction occupied by the phase i. The burning of different ions i and j occurs on interfaces between corresponding domains. Roughly, in a BIM with spherical bubbles containing N less abundant ions (i or j), the OCP reaction rate ii can be diluted with respect to the rate in a uniformly mixed state by a factor of $1/N^{2/3}$ (because the reactions occur on interfaces).

Pycnonuclear burning in a lattice can be drastically affected by lattice impurities and imperfections (see, e.g., Ref. [8]). We expect that the effect of impurities or imperfections can be included in Eq. (33) if we treat them as members of the MCP. Because the burning is mainly regulated by the parameter $\widetilde{\lambda}_{ij}$, the rate should be extremely sensitive to variations of equilibrium distances and oscillation frequencies for the reacting nuclei [see Eq. (29)]. Small variations can induce exponentially huge jumps or drops of the Coulomb tunneling probability (for instance, in response to the decrease or increase of inter-ion separations). The impurities and imperfections may be rare, but they may give the leading contribution into the reaction rate.

Moreover, different pairs ij in an MCP may be exposed to different local conditions and have different separations and oscillator frequencies. One can incorporate these effects by introducing the averaging $\langle \ldots \rangle_{\rm av}$ over an ensemble of such pairs in Eq. (25).

For illustration, we show in Fig. 3 the density dependence of C+C, C+O, and O+O pycnonuclear reactions in carbon-oxygen BIMs. The astrophysical factors are taken from Sec. II. In the main part of the figure, we use the optimal reaction model from Table II. The dot-and-dashed lines show the C+C burning in a pure carbon matter ($x_{\rm C} = 1$) and O+O burning in a pure oxygen matter ($x_{\rm C} = 0$), while other lines are for the C-O mixture with $x_{\rm C} = \frac{1}{2}$. The solid lines present the reaction rates in the uniform C-O mixture. For the C+C and O+O reactions, these lines go slightly lower than the dash-and-dot lines because of the reduced amount of carbon and oxygen in a BIM (as compared to pure carbon or oxygen matter). The long-dashed lines give the reaction rates in the bcc C-O regular crystal. The C+O burning in this crystal has the same rate as in the C-O uniform mix (the solid line) in our model. To illustrate the blocking effect (produced by the absence of closest CC or OO neighbors in the crystal), we calculated the C+C and O+O reaction rates using Eq. (33) but we increased the distances between the reacting nuclei in Eq. (28) by a factor of $\alpha_{dii} = 2/\sqrt{3}$, where $i =$ C or O (see above). Because the local oscillator frequencies for these CC and OO pairs are unknown, we assumed the ion-sphere rescaling ($\alpha^2_{\omega ii} = 1/\alpha^3_{dii}$). The blocking effect is strong, reducing the reaction rates by 5–7 orders of magnitude. Nevertheless, even with this blocking, the C+C reaction is much faster than the C+O and O+O ones because of a much lower Coulomb barrier. Finally, we also calculated the BIM reaction rates assuming phase separation of C and O. We did not plot the respective C+C and O+O reaction rates because they are almost indistinguishable from the corresponding dot-and-dashed lines (the rates are only twice lower than those in the respective OCPs). However, the C+O burning in this case can be strongly suppressed because it occurs only at interfaces between separated phases. For example, the dotted line shows such a C+O burning rate assuming separation into domains which contain 10^6 ions.

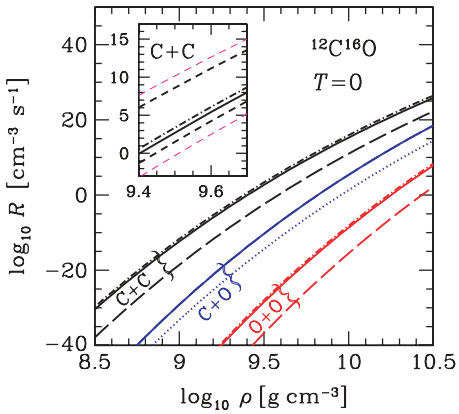

FIG. 3. (Color online) Rates of pycnonuclear C+C, C+O, and O+O reactions vs density for the optimal burning model. Dot-and-dashed lines show C+C burning in a pure carbon crystal and O+O burning in a pure oxygen crystal. Other lines are for the C-O mixture ($x_{\rm C} = 0.5$); solid lines refer to a uniform BIM; long-dashed lines are for a regular C-O bcc crystal; dots are for phase-separated matter. Inset shows the same curves for the C+C reaction on a larger scale; thicker short-dashed lines give the maximum and minimum reaction rates for the uniform C-O mixture in the ion-sphere model ($\alpha_\lambda = 1$); thin short-dashed lines are the same but allow for the variation of α_λ (see text for details).

The inset in Fig. 3 displays the C+C reaction rate on a larger scale. The solid and dot-and-dashed lines are the same as in the main part of the figure. Short dashed lines present the maximum and minimum reaction rates for the uniform C-O mixture; they reflect uncertainties of existing theoretical models for pycnonuclear burning. These lines are calculated using the parameters from Table II. Thicker short-dashed lines give the maximum and minimum reaction rates using the ion-sphere model (neglecting deviations from the ion-sphere rescaling; i.e., assuming $\alpha_{\lambda \rm CC} = 1$). Thinner short-dashed lines are the estimated maximum and minimum reaction rates taking into account possible deviations from the ion-sphere model. The current theoretical uncertainties of the reaction rate are really large.

E. Thermally enhanced pycnonuclear regime

This regime operates in the temperature range $0.5\, T^{(p)}_{ij} / \ln(T^{(l)}_{ij}/T^{(p)}_{ij}) \lesssim T \lesssim 0.5\, T^{(p)}_{ij}$ (see Ref. [8]). At these temperatures, the majority of nuclei occupy ground states in their potential wells, but the main contribution to the reaction rate comes from a small amount of nuclei which occupy excited bound states. This regime is difficult for theoretical studies. We will follow the approach of Ref. [11], which is based on an analytical approximation of the WKB calculations performed by Salpeter and Van Horn [8]. We generalize this approach to an MCP in the same manner as in Sec. III D, by rescaling λ

and T_p in accordance with Eqs. (12) and (10). In this case,

$$\frac{R_{ij}^{\rm pyc}(T)}{R_{ij}^{\rm pyc}(0)} - 1 = \frac{\Omega}{\widetilde{\lambda}_{ij}^{1/2}} \exp\left[-\Lambda\,\frac{\widetilde{T}_{ij}^{(p)}}{T} + \frac{\Omega_1}{(\widetilde{\lambda}_{ij})^{1/2}} \exp\left(-\frac{\Lambda \widetilde{T}_{ij}^{(p)}}{T}\right)\right], \quad (34)$$

where $\widetilde{T}_{ij}^{(p)} \equiv \hbar\omega_{ij}/k_B = \alpha_{\omega ij} T_{ij}^{(p)}$, while Ω, Ω_1, and Λ are model-dependent dimensionless constants. We adopt $\alpha_{\omega ij} = 0.95$ to maximize the reaction rate and $\alpha_{\omega ij} = 1.05$ to minimize it (Table II). In analogy with Ref. [11], the characteristic energy of the reacting nuclei can be taken in the form

$$E_{ij}^{\rm pk} \approx \hbar\omega_{ij} + \frac{Z_i Z_j e^2}{a_{ij}} \exp\left(-\Lambda\,\frac{\widetilde{T}_{ij}^{(p)}}{T}\right). \quad (35)$$

The first term is the reaction energy in the zero-temperature pycnonuclear regime, while the second term describes an increase of $E_{ij}^{\rm pk}$ with growing temperature in the thermally enhanced pycnonuclear regime. Equation (35) is approximate (based on the results of Ref. [8] as explained in [11]), but we expect that it correctly reflects the main features of the accurate expression (to be derived in future, more elaborate calculations). The analogous expression (26) for OCP in Ref. [11] contains two new free factors, C_1 and C_2, in the first and second terms, respectively. They were set $C_1 = C_2 = 1$ in numerical calculations [11] because the theory [8] is insufficiently precise to determine them. We do not introduce these factors here to avoid additional unknowns, but they could be introduced in the future. An uncertainty in $E_{ij}^{\rm pk}$ should not greatly affect the reaction rates.

After Salpeter and Van Horn [8], the thermally enhanced pycnonuclear burning in an OCP was studied by Kitamura and Ichimaru [53] assuming that the reacting nuclei move in an angle-averaged, radial static mean-field potential determined from Monte Carlo sampling of classical Coulomb systems. Although this approach is less justified than the WKB approximation of Ref. [8], the results are in a reasonable agreement (see Ref. [11] for details). Kitamura [47] generalized the results of Ref. [53] to the case of BIMs using the ion-sphere rescaling rule ($\alpha_{\lambda ij} = \alpha_{\omega ij} = 1$).

The thermally enhanced pycnonuclear burning is as sensitive to the microphysical structure of the MCP as is the zero-temperature pycnonuclear burning (Sec. III D). The above comments refer to a uniformly mixed MCP. In the case of a regular MCP lattice, the reaction will be suppressed by the same blocking effects as discussed in Sec. III D. The case of phase separation has the same features as at $T = 0$. Illustrative examples will be given in Sec. IV.

F. The intermediate thermo-pycnonuclear regime

The thermo-pycnonuclear regime is realized at temperatures $T_{ij}^{(p)}/2 \lesssim T \lesssim T_{ij}^{(p)}$ which separate the domains of classical and quantum motion of the reacting nuclei. The calculation of the reaction rate in this regime is very complicated. We will describe this rate by a phenomenological expression presented below.

The reaction is mainly determined by the nuclei that become slightly unbound and can move freely through the dense matter, fusing not only with the closest neighbors (pycnonuclear regime), but also with other nuclei (thermonuclear regime). We expect that the transition from the pycnonuclear to the thermonuclear regime with the growth of temperature in a uniformly mixed MCP is sufficiently smooth. When the number of freely reacting nuclei becomes large, the dependence of the reaction rate on the details of the MCP microstructure should disappear.

G. Single analytical approximation in all regimes

Our phenomenological expression for the temperature- and density-dependent reaction rate, which combines all five burning regimes and *assumes a uniformly mixed MCP at low temperatures*, is a straightforward generalization of the expression for the OCP considered in Ref. [11],

$$\begin{aligned} R_{ij}(\rho,T) &= R_{ij}^{\rm pyc}(\rho) + \Delta R_{ij}(\rho,T), \\ \Delta R_{ij}(\rho,T) &= \frac{n_i n_j}{1+\delta_{ij}} \frac{S\left(E_{ij}^{\rm pk}\right)}{\hbar} r_{{\rm B}ij} P F, \\ F &= \exp\left(-\widetilde{\tau}_{ij} + C_{\rm sc}\widetilde{\Gamma}_{ij}\varphi \right. \\ &\quad \left. \times \exp\left(-\Lambda \widetilde{T}_{ij}^{(p)}/T\right) - \Lambda \frac{\widetilde{T}_{ij}^{(p)}}{T}\right), \\ P &= \frac{8\pi^{1/3}}{\sqrt{3}\,2^{1/3}} \left(\frac{E_{ij}^{\rm a}}{k_B \widetilde{T}}\right)^{\gamma}. \end{aligned} \quad (36)$$

In this case, $\varphi = \sqrt{\Gamma_{ij}}/[(C_{ij}^{\rm sc}/\zeta_{ij})^4 + \Gamma_{ij}^2]^{1/4}$; $R_{ij}^{\rm pyc}(\rho)$ is the density-dependent pycnonuclear reaction rate at zero temperature discussed in Sec. III D; $\Delta R_{ij}(\rho,T)$ is the density- and temperature-dependent part including an exponential function F and a pre-exponent P. The quantities $\widetilde{\tau}_{ij}$ and $\widetilde{\Gamma}_{ij}$ are similar to the familiar quantities τ_{ij} and Γ_{ij}, but they contain a "renormalized" temperature $\widetilde{T}$,

$$\begin{aligned} \widetilde{\tau}_{ij} &= 3\left(\frac{\pi}{2}\right)^{2/3} \left(\frac{E_{ij}^{a}}{k_B \widetilde{T}}\right)^{1/3}, \\ \widetilde{\Gamma}_{ij} &= \frac{Z_i Z_j e^2}{a_{ij} k_B \widetilde{T}}, \quad \widetilde{T} = \sqrt{T^2 + C_T^2 \left(T_{ij}^{(p)}\right)^2}, \end{aligned} \quad (37)$$

where C_T is a dimensionless renormalization parameter specified below. Equations (36) and (37) are analogous to Eqs. (27) and (28) of Ref. [11]. The term $\Delta R_{ij}(\rho,T)$ and the renormalized temperature $\widetilde{T}$ are introduced to match the equations in thermonuclear and pycnonuclear regimes. The renormalized temperature reflects the fact that the thermal energy $k_B T$ of plasma ions in the thermonuclear case is replaced by a temperature-independent zero-point energy in the pycnonuclear case.

For high temperatures $T \gg T_{ij}^{(p)}$, we have $\widetilde{\tau}_{ij} \to \tau_{ij}$, $\widetilde{\Gamma}_{ij} \to \Gamma_{ij}$, and $\widetilde{T} \to T$. In this case, $\Delta R_{ij}(\rho,T) \to R_{ij}^{\rm th}(\rho,T) \gg$

$R_{ij}^{\rm pyc}(\rho)$, and Eq. (36) reproduces the thermonuclear reaction rate (Secs. III B and III C). At low temperatures $T \lesssim T_{ij}^{(p)}$, the quantities $\widetilde{\tau}_{ij}$, $\widetilde{\Gamma}_{ij}$, and $\widetilde{T}$ contain the "quantum" temperature $T_{ij}^{(p)}$, determined by zero-point ion vibrations, rather than the real temperature T. In the limit of $T \to 0$, we obtain $\widetilde{\Gamma}_{ij} = 1/[(\lambda_{ij})^{1/2}\,(72\pi)^{1/6} C_T]$ and $\widetilde{\tau}_{ij} = 3(\pi/\lambda_{ij})^{1/2}/(2^{7/6}\,C_T^{1/3})$.

Following Ref. [11], we require that at $T \ll T_{ij}^{(p)}$ the factor $\exp(-\widetilde{\tau}_{ij})$ in the exponential function F, Eq. (36), reduces to $\exp[-C_{\rm exp}/(\widetilde{\lambda}_{ij})^{1/2}]$. This would allow us to obey Eq. (34) by satisfying the equality

$$3\sqrt{\pi}/\left(2^{7/6}C_T^{1/3}\right) = C_{\rm exp}(\alpha_{\lambda ij})^{-1/2}. \tag{38}$$

The double-exponent factor in F, Eq. (36), will correspond to the double-exponent factor in Eq. (34). Taking $C_{\rm exp}$ and $\alpha_{\lambda ij}$ from Table II, we can determine C_T. These parameters are also listed in Table II. In the MCP they are different from those in the OCP because in the MCP we introduce an additional parameter $\alpha_{\lambda ij}$ (Sec. III D). The values of C_T for the OCP [11] are given in Table II in parentheses.

Finally, the quantity γ in Eq. (36) and the reaction energy $E_{ij}^{\rm pk}$ in the astrophysical factor $S(E_{ij}^{\rm pk})$ can be chosen in the same way as in Ref. [11],

$$\gamma = \left[T^2\gamma_1 + \left(\widetilde{T}_{ij}^{(p)}\right)^2\gamma_2\right]/\left[T^2 + \left(\widetilde{T}_{ij}^{(p)}\right)^2\right], \tag{39}$$

$$E_{ij}^{\rm pk} = \hbar\widetilde{\omega}_{ij}^{(p)} + \left(\frac{Z_i Z_j e^2}{a_{ij}} + \frac{k_{\rm B}T\tau_{ij}}{3}\right)\exp\left(-\frac{\Lambda\widetilde{T}_{ij}^{(p)}}{T}\right), \tag{40}$$

where $\gamma_1 = 2/3$ and $\gamma_2 = (2/3)\,(C_{\rm pl} + 0.5)$.

Thus, we propose to use the analytic expression (36) for the reaction rate in a uniformly mixed MCP with the following parameters:

(i) The parameter $C_{\rm sc}$ of strongly screened thermonuclear burning is given by Eq. (21).

(ii) The parameters $C_{\rm exp}$, $C_{\rm pyc}$, $C_{\rm pl}$, $\alpha_{\lambda ij}$ of zero-temperature pycnonuclear burning, and the parameters $\alpha_{\omega ij}$, Λ, and C_T of thermally enhanced pycnonuclear burning are given in Table II.

In this way, we obtain (Table II) three models for any given nonresonant nuclear fusion reaction (9) in a uniformly mixed MCP. One is the optimal model, the second gives the maximum reaction rate, and the third gives the minimum reaction rate. For the OCP, it is sufficient to set $\alpha_{\lambda ij} = \alpha_{\omega ij} = 1$, which reduces the present results to those of Ref. [11].

The uncertainties of the reaction rate become larger if a cold MCP forms a regular lattice or undergoes a phase separation or contains impurities and defects. All these cases can be approximately taken into account in the same way as discussed in Sec. III D. For instance, a reaction in a regular lattice can be strongly blocked by the absence of the closest reacting neighbors (Secs. III D and III E; also see Sec. IV).

Our formula for a uniformly mixed MCP gives a smooth behavior of the reaction rate as a function of temperature and density, without jumps at the solidification point (in analogy with an OCP, see Ref. [11]). In the cases of other MCP microstructures, such jumps may appear.

Our formula is flexible. Its parameters could be tuned when new microscopic calculations of reaction rates appear in the future. Moreover, the formula can be improved even if new information on MCP properties (not on reaction rates directly) appear in the literature (for instance, on the deviations from the ion-sphere scaling at $T = 0$).

More complicated expressions for the reaction rates in the OCP and uniform BIMs were proposed by Kitamura [47]. His expressions are mainly based on the results of Refs. [45, 46,48,51,53] (in the different regimes) which are not free of approximations (see Ref. [11] for details). His expressions for BIMs are obtained assuming the ion-sphere rescaling rule ($\alpha_{\lambda ij} = \alpha_{\omega ij} = 1$) and are, therefore, more restricted than our expression. Their derivation implies that they are valid for uniformly mixed BIMs. In particular, they do not take into account blocking effects in regular binary lattices.

In contrast to our formula, Kitamura took into account the effects of electron screening (finite polarizability of the electron gas). However, these effects are relatively weak; their strict inclusion in the pycnonuclear regime is complicated. We do not include them but, instead, take into account theoretical uncertainties of the reaction rates without electron screening. The results of Kitamura [47] for an OCP lie well within these uncertainties. His results for BIMs in the thermonuclear regime with strong screening and essentially different charges of reacting nuclei are less accurate than our results (Sec. III C).

IV. NUCLEAR BURNING IN A CARBON-OXYGEN MIXTURE

To illustrate our results, we analyze nuclear reactions in a dense ^{12}C-^{16}O mixture. Figure 4 shows the temperature

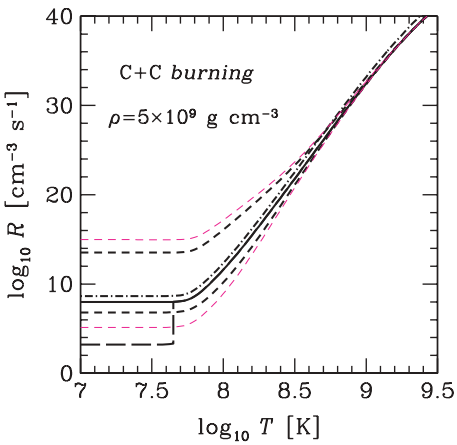

FIG. 4. (Color online) C+C reaction rate vs temperature at $\rho = 5 \times 10^9$ g cm^{-3}. Dot-and-dashed line is the optimal model for pure carbon matter; other lines are for a C-O mixture with $x_{\rm C} = 0.5$. Solid line is the optimal model for a uniform mixture; long-dashed line is for the regular bcc C-O crystal at low temperatures (vertical part indicates the melting point). Thicker short-dashed lines give the maximum and minimum reaction rates for the uniform C-O mixture in the ion-sphere model ($\alpha_\lambda = 1$); thinner short dashed-lines are the same but allow for deviations from the ion-sphere model (see text for details).

dependence of the C+C reaction rate at $\rho = 5 \times 10^9$ g cm^{-3} (for the same reaction models as in Fig. 3). The dot-and-dashed line is the optimal model (Table II) for a pure carbon matter (from Ref. [11]). Other lines are for C-O mixtures with equal numbers of C and O nuclei ($x_C = \frac{1}{2}$). The solid line is the optimal model for the uniform mixture; the thicker short-dashed lines show the maximum and minimum reaction rates in such a mixture in the ion-sphere approximation ($\alpha_{\lambda CC} = \alpha_{\omega CC} = 1$); the thinner short-dashed lines are the same but beyond the ion-sphere approximation (note that variations of $\alpha_{\omega CC}$ appear to be much less important than variations of $\alpha_{\lambda CC}$). The long-dashed line is for a C-O regular lattice (in the same approximation as used in Fig. 3). A sharp jump in this curve is associated with the melting of the crystal (Fig. 2), which destroys the blocking of the C+C burning and amplifies the reaction rate.

Figure 4 shows the reaction rates in all burning regimes (except for the classical thermonuclear burning which would require higher temperatures; see Fig. 2). The horizontal parts of the curves for $\log T\,[\mathrm{K}] \lesssim 7.7$ refer to the zero-temperature pycnonuclear burning; the respective reaction rates are independent of T as discussed in Sec. III D and displayed in Fig. 3. The temperature range $7.7 \lesssim \log T\,[\mathrm{K}] \lesssim 8.3$ corresponds to the thermally enhanced pycnonuclear regime. The reaction rate starts to grow with increasing T (Sec. III E). The rate remains highly uncertain for the same reasons as in the zero-temperature pycnonuclear regime. The next temperature range $8.3 \lesssim \log T\,[\mathrm{K}] \lesssim 8.6$ corresponds to the intermediate thermo-pycnonuclear burning (Sec. III F). Theoretical uncertainties of the reaction rate become smaller. Finally, the temperature range $\log T\,[\mathrm{K}] \gtrsim 8.6$ refers to the thermonuclear burning with strong plasma screening. The theoretical uncertainties become much smaller although the enhancement of the reaction rate by the plasma screening effects is huge; with increasing T this enhancement weakens and the reaction rate matches the classical thermonuclear rate (see Fig. 6 of Ref. [11]). The presence of oxygen slightly reduces the C+C reaction rate (by reducing the amount of carbon nuclei at a given density).

Based on our expression for the reaction rates, we plot in Fig. 2 the T-ρ domains (shaded strips), where the C+C, C+O, and O+O reactions are most important. The domains for the C+C and O+O reactions are presented for pure carbon or pure oxygen matter ($x_C = 1$ and $x_C = 0$, respectively). For the C+O reaction, we have taken the C-O mixture with $x_C = \frac{1}{2}$. A domain for any reaction ij is restricted by two lines along which the characteristic burning time $\tau_i = n_i / R_{ij}$ of nuclei i is constant (taken to be 10^6 years for a lower line and 1 year for an upper line, for example). Above the upper line, the reaction ij is so fast that the nuclei i cannot survive for a long time. Below the lower line, the reaction is so slow that the nuclei i survive almost forever. Therefore, the strips represent the temperature and density domains of greatest relevance for the carbon and oxygen nucleosynthesis through the reactions under discussion. For determining these domains, we have taken the optimal model from Table II. The domains do not change significantly under variations of fractional numbers of C and O within reasonable limits. For densities $\rho \lesssim 10^9$ g cm^{-3}, the strips

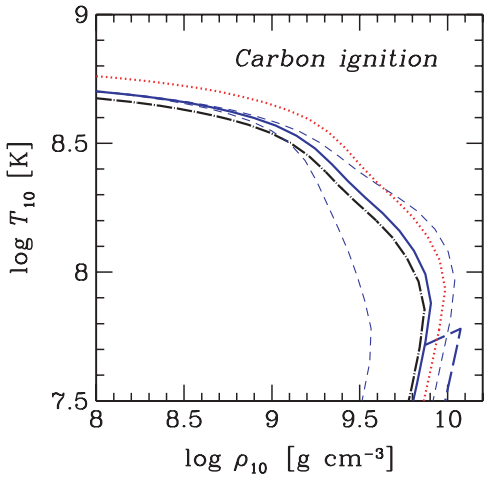

FIG. 5. (Color online) Carbon ignition curves in ^{12}C-^{16}O matter. Dot-and-dashed line is the optimal model for carbon burning in pure carbon matter. Solid and dotted lines are optimal models for uniform C-O mixtures with $x_C = 0.5$ and 0.1, respectively. Other lines are for C-O BIMs with $x_C = 0.5$. Short-dashed lines give the highest and lowest theoretical ignition curves for uniform mixtures. Long-dashed line is for the C-O bcc crystal at low temperatures.

are almost horizontal; nuclear burning in them proceeds in the thermonuclear regime, and the reaction rates depend mainly on the temperature. In contrast, the strips become almost vertical at low temperatures, reflecting the pycnonuclear burning regime where the reaction rates depend mainly on the density.

The strips show a strong heterogeneity of the different reactions. It is evidently caused by different heights of Coulomb barriers. With increasing ρ and/or T in the C-O matter, carbon will burn first in the C+C reaction and could be burnt almost completely before reaching the T-ρ domain, where the C+O reaction can be efficient.

Finally, we have studied the carbon ignition curve, which is a necessary ingredient for modeling nuclear explosions of massive white dwarfs (supernova Ia events) and carbon explosions in accreting neutron stars (superbursts). The ignition curve is usually determined as the line in the T-ρ plane (Fig. 5), where the nuclear energy generation rate equals the local neutrino energy losses. At higher T and ρ (above the curve), the nuclear energy generation exceeds the neutrino losses (which cool the matter) and carbon ignites. We have calculated such curves for C-O mixtures. All reactions (C+C, C+O, and O+O) have been taken into account but the C+O and O+O reactions have appeared to be unimportant owing to the heterogeneity of nuclear burning. The presence of oxygen affects carbon ignition only through the C+C reaction rate and the neutrino emission rate. The neutrino energy losses have been assumed to be produced by plasmon decay and by electron-nucleus bremsstrahlung. The neutrino emissivity owing to plasmon decay has been obtained from extended tables calculated by M. E. Gusakov (unpublished); they are in good agreement with the results of Itoh *et al.* [54]. The neutrino bremsstrahlung emissivity has been calculated using the formalism of Kaminker *et al.* [55], which takes into account electron band

structure effects in crystalline matter. For a C-O mixture, this neutrino emissivity has been determined using the linear mixture rule.

The dot-and-dashed line in Fig. 5 shows the carbon ignition curve, calculated using the optimal model of carbon burning in pure carbon matter ($x_C = 1$; from Ref. [11]). The solid and dotted lines are the same curves in C-O mixtures with $x_C = 0.5$ and 0.1, respectively (assuming the optimal reaction model and a uniform mixture at low temperatures). At $\rho \lesssim 10^9$ g cm^{-3}, the curves depend weakly on the density because carbon burns in the thermonuclear regime. At $T \lesssim 10^8$ K, the curves depend weakly on the temperature because carbon burns in the pycnonuclear regime. A strong bending of the curves in the density range from $\sim 10^9$ to $\sim 3 \times 10^9$ g cm^{-3} is associated with the transition from thermonuclear burning to pycnonuclear. As the carbon fraction decreases, the ignition curve shifts to higher T and ρ, mainly because of the drop in the C+C reaction rate.

The short-dashed lines in Fig. 5 show the uncertainty of the solid ignition curve ($x_C = \frac{1}{2}$, a uniform C-O mixture) associated with the uncertainties of the reaction rates (assuming the maximum and minimum reaction rates from Table II). In the thermonuclear regime, the uncertainties are small; while in the pycnonuclear regime, they are substantial. The long-dashed line shows the ignition curve calculated under the assumption that a regular bcc C-O lattice is formed in the C-O mixture ($x_C = \frac{1}{2}$) after the crystallization. The blocking of the C+C reaction rate by oxygen ions in the bcc lattice shifts the ignition curve to higher ρ. The sudden break in this line is associated with the crystallization (analogous to the break in the long-dashed line in Fig. 4).

The carbon ignition curve obtained by equating the nuclear energy generation and the neutrino losses becomes unreliable for $T \lesssim 10^8$ K (e.g., Ref. [11]). The main reason is that this curve falls in the T-ρ domain, where the characteristic carbon burning time is unrealistically large (exceeds the age of the universe). In addition, the neutrino emission becomes a very slow, inefficient means for carrying away the nuclear energy; thermal conduction can be much more efficient. As a result, the carbon ignition condition becomes nonlocal, complicated, and dependent on a specific model (a neutron star, white dwarf, etc.).

V. CONCLUSIONS

We have studied the problem of Coulomb barrier penetration for nonresonant nuclear fusion reactions in a dense MCP of atomic nuclei. We have considered all five nuclear burning regimes (Secs. III B–III F) and analyzed calculations of nuclear reaction rates in an MCP for these regimes, available in the literature. We have proposed (Sec. III G) a unified phenomenological expression for the reaction rate valid for all regimes. It generalizes an analogous expression proposed recently [11] for an OCP. The expression contains several parameters which can be varied to account for current theoretical uncertainties of the reaction rates.

Our main conclusions are the following:

(i) The reaction rates in the thermonuclear regimes (with weak and strong plasma screening) can be calculated sufficiently accurately. In the regime of strong screening and for reacting nuclei with nonequal charges, our expression is more accurate than those proposed in the literature (Sec. III C).

(ii) The reaction rates in other regimes (zero-temperature and thermally enhanced pycnonuclear regimes; intermdiate thermo-pycnonuclear regime) are much less certain. They are very sensitive to currently unknown microphysical correlation properties in an MCP (a uniform mix, a regular crystalline lattice, a phase-separated matter, a matter with impurities and defects); they are much richer in physics than those in the OCP case.

(iii) At low temperatures, we have mainly considered reactions in a uniform mix. Other MCP microstructures can strongly decrease or increase the reaction rates. For instance, the reactions in a regular MCP lattice can be strongly suppressed by the absence of nearby reacting nuclei.

(iv) Our phenomenological expression can be improved (Sec. III G) after new calculations of the reaction rates or main properties of the MCP are performed. It would be important to know the actual microstructure of the MCP at low temperatures (first of all, the availability of closest neighbors, local separations, and oscillation frequencies of neighboring nuclei, particularly in the presence of impurities and lattice defects).

(v) Although our main formula in Sec. III G assumes a uniform mix at low T, the presented results are sufficient to understand qualitatively the reaction rates for other cases (following the prescriptions of Sec. III D).

For illustration, we have considered (Sec. IV) C+C, C+O, and O+O nuclear reactions in a dense carbon-oxygen mixture, which is important for the structure and evolution of massive white dwarfs (supernova Ia explosions) and accreting neutron stars (as sources of superbursts). For this purpose, we have calculated and parametrized the appropriate astrophysical factors (Sec. II). The main results of our analysis are as follows:

(i) The ranges of densities and temperatures at which the C+C, C+O, and O+O reactions are very important look like narrow regions in the temperature-density diagram (Fig. 2); the regions do not strongly overlap, which means a strong heterogeneity of these reactions.

(ii) With increasing density and/or temperature, carbon starts burning first in the C+C reaction (because carbon nuclei have a lower Coulomb barrier); this reaction is very important in the nuclear evolution of C-O mixtures.

(iii) Carbon burning in the C+C reaction is affected by the presence of oxygen. The effect is simple in the thermonuclear regimes but more complicated in other regimes (at low temperatures).

(iv) Carbon ignition in a C-O mixture occurs (Fig. 5) in thermonuclear regimes as long as $\rho \lesssim 10^9$ g cm^{-3} (and $T \gtrsim 3 \times 10^8$ K). It can be calculated quite accurately. With the decrease of carbon fraction, the ignition curve shifts to higher ρ and T.

(v) At $\rho \gtrsim 10^9$ g cm^{-3} and $T \lesssim 3 \times 10^8$ K the ignition condition becomes uncertain (Sec. IV). The formation of a regular C-O lattice after crystallization can block the C+C reaction and shift carbon ignition to higher densities.

Our consideration in this paper was general. More quantitative nuclear network simulations involving thermonuclear and pycnonuclear burning in dense stellar matter are currently in progress.

ACKNOWLEDGMENTS

We are grateful to H. E. DeWitt for comments and suggestions and to M. E. Gusakov for providing the tables of neutrino emissivities caused by plasmon decay. This work was partially supported by the Joint Institute for Nuclear Astrophysics (NSF PHY 0216783), the Russian Foundation for Basic Research (Grant Nos. 05-02-16245, 05-02-22003), and the Federal Agency for Science and Innovations (Grant No. NSh 9879.2006.2).

[1] M. F. El Eid, B. S. Meyer, and L.-S. The, Astrophys. J. **611**, 452 (2004).
[2] R. C. Pardo, R. G. Couch, and W. D. Arnett, Astrophys. J. **191**, 711 (1974).
[3] J. W. Truran and W. D. Arnett, Astrophys. J. **160**, 181 (1970).
[4] J. C. Niemeyer and S. E. Woosley, Astrophys. J. **475**, 740 (1997).
[5] T. Strohmeyer and L. Bildsten, in *Compact Stellar X-Ray Sources*, edited by W. H. G. Lewin and M. Van der Klis (Cambridge University, Cambridge, 2006), p. 113.
[6] A. Cumming, J. Macbeth, J. J. M. in 't Zand, and D. Page, Astrophys. J. **646**, 429 (2006).
[7] D. Page and A. Cumming, Astrophys. J. **635**, L157 (2005).
[8] E. E. Salpeter and H. M. Van Horn, Astrophys. J. **155**, 183 (1969).
[9] S. Schramm and S. E. Koonin, Astrophys. J. **365**, 296 (1990); **377**, 343E (1991).
[10] P. Haensel and J. L. Zdunik, Astron. Astrophys. **229**, 117 (1990); **404**, L33 (2003).
[11] L. R. Gasques, A. V. Afanasjev, E. F. Aguilera, M. Beard, L. C. Chamon, P. Ring, M. Wiescher, and D. G. Yakovlev, Phys. Rev. C **72**, 025806 (2005).
[12] W. A. Fowler, G. R. Caughlan, and B. A. Zimmerman, Annu. Rev. Astron. Astrophys. **13**, 69 (1975).
[13] D. D. Clayton, *Principles of Stellar Evolution and Nucleosynthesis* (University of Chicago, Chicago, 1983).
[14] E. E. Salpeter, Aust. J. Phys. **7**, 373 (1954).
[15] L. R. Gasques, L. C. Chamon, D. Pereira, M. A. G. Alvarez, E. S. Rossi Jr., C. P. Silva, and B. V. Carlson, Phys. Rev. C **69**, 034603 (2004).
[16] M. A. Cândido Ribeiro, L. C. Chamon, D. Pereira, M. S. Hussein, and D. Galetti, Phys. Rev. Lett. **78**, 3270 (1997).
[17] L. C. Chamon, D. Pereira, M. S. Hussein, M. A. Cândido Ribeiro, and D. Galetti, Phys. Rev. Lett. **79**, 5218 (1997).
[18] L. C. Chamon, D. Pereira, and M. S. Hussein, Phys. Rev. C **58**, 576 (1998).
[19] L. C. Chamon, B. V. Carlson, L. R. Gasques, D. Pereira, C. De Conti, M. A. G. Alvarez, M. S. Hussein, M. A. Cândido Ribeiro, E. S. Rossi Jr., and C. P. Silva, Phys. Rev. C **66**, 014610 (2002).
[20] M. A. G. Alvarez *et al*., Phys. Rev. C **65**, 014602 (2002).
[21] L. R. Gasques, L. C. Chamon, C. P. Silva, D. Pereira, M. A. G. Alvarez, E. S. Rossi Jr., V. P. Likhachev, B. V. Carlson, and C. De Conti, Phys. Rev. C **65**, 044314 (2002).
[22] E. S. Rossi Jr., D. Pereira, L. C. Chamon, C. P. Silva, M. A. G. Alvarez, L. R. Gasques, J. Lubian, B. V. Carlson, and C. De Conti, Nucl. Phys. **A707**, 325 (2002).
[23] C. A. Barnes, *Essays in Nuclear Astrophysics*, edited by C. A. Barnes, D. D. Clayton, and D. N. Schramm (Cambridge University, Cambridge, 1982), p. 193.
[24] J. R. Patterson, H. Winkler, and C. S. Zaidins, Astrophys. J. **157**, 367 (1969).
[25] M. G. Mazarakis and W. E. Stephens, Phys. Rev. C **7**, 1280 (1973).
[26] M. D. High and B. Cujec, Nucl. Phys. **A282**, 181 (1977).
[27] P. Rosales *et al*., Rev. Mex. Fís. **49**, 88 (2003).
[28] K. U. Kettner, H. Lorenz-Wirzba, and C. Rolfs, Z. Phys. A **298**, 65 (1980).
[29] H. W. Becker *et al*., Z. Phys. A **303**, 305 (1981).
[30] P. R. Christensen, Z. E. Switkowski, and R. A. Dayras, Nucl. Phys. **A280**, 189 (1977).
[31] B. Cujec and C. A. Barnes, Nucl. Phys. **A266**, 461 (1976).
[32] G. Hulke, C. Rolfs, and H.-P. Trautvetter, Z. Phys. A **297**, 161 (1980).
[33] A. Kuronen, J. Keinonen, and P. Tikkanen, Phys. Rev. C **35**, 591 (1987).
[34] S.-C. Wu and C. A. Barnes, Nucl. Phys. **A422**, 373 (1984).
[35] D. G. Kovar *et al*., Phys. Rev. C **20**, 1305 (1979).
[36] J. Thomas, Y. T. Chen, S. Hinds, D. Meredith, and M. Olson, Phys. Rev. C **33**, 1679 (1986).
[37] H. E. DeWitt, W. Slattery, D. Baiko, and D. Yakovlev, Contrib. Plasma Phys. **41**, 251 (2001).
[38] H. E. DeWitt, W. L. Slattery, and J. Yang, in *Strongly Coupled Plasma Physics*, edited by H. M. Van Horn and S. Ichimaru (University of Rochester, Rochester, 1993), p. 425.
[39] H. DeWitt and W. Slattery, Contrib. Plasma Phys. **43**, 279 (2003).
[40] S. Ichimaru, Rev. Mod. Phys. **54**, 1017 (1982).
[41] H. E. DeWitt, H. C. Graboske, and M. S. Cooper, Astrophys. J. **181**, 439 (1973).
[42] B. Jancovici, J. Stat. Phys. **17**, 357 (1977).
[43] R. Mochkovitch and K. Nomoto, Astron. Astrophys. **154**, 115 (1986); **157**, 403E (1986).
[44] H. DeWitt and W. Slattery, Contrib. Plasma Phys. **39**, 97 (1999).
[45] S. Ogata, H. Iyetomi, and S. Ichimaru, Astrophys. J. **372**, 259 (1991).

[46] S. Ogata, S. Ichimaru, and H. M. Van Horn, Astrophys. J. **417**, 265 (1993).
[47] H. Kitamura, Astrophys. J. **539**, 888 (2000).
[48] S. Ogata, Astrophys. J. **481**, 883 (1997).
[49] Y. Rosenfeld, Phys. Rev. E **53**, 2000 (1996).
[50] Y. Rosenfeld, Phys. Rev. E **54**, 2827 (1996).
[51] S. Ichimaru, S. Ogata, and H. M. Van Horn, Astrophys. J. **401**, L35 (1992).
[52] S. Ogata, H. Iyetomi, S. Ichimaru, and H. M. Van Horn, Phys. Rev. E **48**, 1344 (1993).
[53] H. Kitamura and S. Ichimaru, Astrophys. J. **438**, 300 (1995).
[54] N. Itoh, H. Mutoh, A. Hikita, and Y. Kohyama, Astrophys. J. **395**, 622 (1992); **404**, 418E (1993).
[55] A. D. Kaminker, C. J. Pethick, A. Y. Potekhin, V. Thorsson, and D. G. Yakovlev, Astron. Astrophys. **343**, 1009 (1999).